AGU PUBLICATIONS

JGR

Journal of Geophysical Research: Atmospheres

RESEARCH ARTICLE

10.1002/2013JD021397

The influence of natural and anthropogenic factors on major stratospheric sudden warmings

F. Hansen[1], K. Matthes[1], C. Petrick[2,3], and W. Wang[1,4]

[1]GEOMAR Helmholtz Centre for Ocean Research Kiel, Kiel, Germany, [2]Formerly at GEOMAR Helmholtz Centre for Ocean Research Kiel, Kiel, Germany, [3]Formerly at GFZ German Research Center for Geosciences, Potsdam, Germany, [4]Institute of Meteorology, Freie Universität Berlin, Berlin, Germany

Key Points:
- The QBO reduces the frequency of major SSWs; SST variability increases it
- Anthropogenic GHGs and ODSs determine the prewarming phase of major SSWs
- Two-way ocean/atmosphere coupling is needed for the negative AO response after SSWs

Correspondence to:
F. Hansen,
fhansen@geomar.de

Citation:
Hansen, F., K. Matthes, C. Petrick, and W. Wang (2014), The influence of natural and anthropogenic factors on major stratospheric sudden warmings, *J. Geophys. Res. Atmos.*, *119*, 8117–8136, doi:10.1002/2013JD021397.

Received 19 DEC 2013
Accepted 18 JUN 2014
Accepted article online 24 JUN 2014
Published online 15 JUL 2014

Abstract Major stratospheric sudden warmings are prominent disturbances of the Northern Hemisphere polar winter stratosphere. Understanding the factors controlling major warmings is required, since the associated circulation changes can propagate down into the troposphere and affect the surface climate, suggesting enhanced prediction skill when these processes are accurately represented in models. In this study we investigate how different natural and anthropogenic factors, namely, the quasi-biennial oscillation (QBO), sea surface temperatures (SSTs), anthropogenic greenhouse gases, and ozone-depleting substances, influence the frequency, variability, and life cycle of major warmings. This is done using sensitivity experiments performed with the National Center for Atmospheric Research's Community Earth System Model (CESM). CESM is able to simulate the life cycle of major warmings realistically. The QBO strengthens the climatological stratospheric polar night jet (PNJ) and significantly reduces the frequency of major warmings through reduction of planetary wave propagation into the PNJ region. Variability in SSTs weakens the PNJ and significantly increases the major warming frequency due to enhanced wave forcing. Even extreme climate change conditions (RCP8.5 scenario) do not influence the total frequency but determine the prewarming phase of major warmings. The amplitude and duration of major warmings seem to be mainly determined by internal stratospheric variability. We also suggest that SST variability, two-way ocean/atmosphere coupling, and hence the memory of the ocean are needed to reproduce the observed tropospheric negative Northern Annular Mode pattern after major warmings.

1. Introduction

Stratospheric sudden warmings (SSWs) are prominent disturbances of the Northern Hemisphere (NH) winter stratospheric polar vortex and are also a clear manifestation of the dynamical coupling in the stratosphere-troposphere system. They were first discovered by *Scherhag* [1952] and are induced by the interaction of upward propagating planetary waves of tropospheric origin with the zonal mean flow [*Matsuno*, 1971]. By this interaction, the vortex is disrupted in its zonal symmetry and displaced from the pole or split into two vortices, leading to increased temperatures in the polar stratosphere. If additionally the wind at 60°N, 10 hPa reverses from westerly to easterly, the warming is called a major warming, according to the definition of the World Meteorological Organization (WMO; *Labitzke and Naujokat* [2000]). The signature of major sudden warmings can descend to the troposphere and thus even affect surface weather and climate [*Quiroz*, 1977; *Baldwin and Dunkerton*, 2001; *Thompson et al.*, 2002; *Mitchell et al.*, 2013]; therefore, the accurate simulation of SSWs and their downward propagating dynamical disturbances yield potential for improving the tropospheric weather prediction skill in climate models [*Baldwin and Dunkerton*, 2001; *Thompson et al.*, 2002; *Mitchell et al.*, 2013].

A major warming is observed about every 2 years [*Erlebach et al.*, 1996; *Labitzke and Naujokat*, 2000; *Charlton and Polvani*, 2007], though *Labitzke* [1977], *Labitzke and Naujokat* [2000], and *Schimanke et al.* [2011] pointed out (in observations and a model study, respectively) that SSW occurrence has large interannual to interdecadal variability. SSWs dominate the interannual variability of the NH polar winter stratosphere [*Labitzke and Naujokat*, 2000]. There are various natural and anthropogenic factors that influence both the mean state and the variability of the polar vortex, suggesting a possible impact of these forcings on SSWs. Natural factors include, e.g., the quasi-biennial oscillation (QBO) of equatorial stratospheric winds, variations in sea surface temperatures (SSTs) such as the El Niño Southern Oscillation (ENSO), the 11 year solar cycle, and volcanic eruptions. Anthropogenic factors involve changes in greenhouse gases

(GHGs) and ozone-depleting substances (ODSs). By affecting either the background winds, the generation and propagation of waves, or the wave-mean flow interaction, these factors impact the polar vortex and hence the frequency and characteristics of SSWs. These dynamical mechanisms are not yet well understood and will be investigated in this study for some of the above mentioned factors.

The influence of the QBO on the polar stratosphere was first examined by *Holton and Tan* [1980, 1982]. On average, the polar stratospheric vortex is colder and less disturbed in QBO west-phase winters, leading to a lower frequency of SSWs, while winters during QBO east phase tend to be warmer and more disturbed, and more SSWs are observed. The mechanism behind this is not fully understood yet; it is likely that both the position of the zero wind line (known as the Holton-Tan mechanism; *Holton and Tan* [1980, 1982]; *Watson and Gray* [2014]) and also the QBO-induced secondary meridional circulation [*Naoe and Shibata*, 2010; *Garfinkel et al.*, 2012] influence the propagation of planetary waves which are then responsible for the stronger or weaker disturbance of the polar vortex.

The influence of SST variations on the polar vortex largely happens within ENSO events. *Van Loon and Labitzke* [1987] found in observations that warm ENSO events (El Niños) seem to be associated with an anomalously weak and warm polar vortex and hence more SSWs. *Manzini et al.* [2006] confirmed in a model study the statistical significance of this relationship and also highlighted its nonlinear character, i.e., that cold ENSO events (La Niñas), on the other hand, do not have an equivalent influence significantly distinguishable from internal variability. This was also confirmed in model studies by, e.g., *Sassi et al.* [2004] and *Taguchi and Hartmann* [2006] and observational studies by *Camp and Tung* [2007] and *Mitchell et al.* [2011]. By analyzing general circulation model simulations, *Manzini et al.* [2006] and *Ayarzagüena et al.* [2013] suggested that the large-scale, extratropical ENSO teleconnection pattern in NH winter includes a deepening of the Aleutian low during El Niño events which enhances the forcing and vertical propagation of quasi-stationary planetary waves, resulting in a weaker stratospheric polar vortex. However, *Butler and Polvani* [2011] and *Garfinkel et al.* [2012] found that the SSW frequency is enhanced during both El Niño and La Niña years in reanalysis data and climate model simulations, despite the opposite-signed influence of the ENSO phases on the polar vortex. In general, two-way coupling between the atmosphere and the ocean in climate models has been shown to increase the low-frequency variability in both media [*Barsugli and Battisti*, 1998]. Recently, *Omrani et al.* [2014] suggested in a model study that decadal variability in North Atlantic SSTs might influence stratospheric background winds and SSWs.

Other natural factors that modify the polar vortex and hence may affect the frequency of SSWs directly or by interaction with other factors are the 11 year solar cycle [e.g., *Gray et al.*, 2010] and volcanic eruptions [e.g., *Robock*, 2000].

The influence of anthropogenic GHGs and ODSs on the polar vortex and SSWs is mainly addressed in model studies using 21st century GHG emission scenarios and comparing them to observations or model simulations of the 20th century. The results are, however, not concordant: while the majority of recent studies shows an increase in SSW frequency under increased GHG forcings [e.g., *Huebener et al.*, 2007; *Charlton-Perez et al.*, 2008; *Bell et al.*, 2009; *Schimanke et al.*, 2013; *Ayarzagüena et al.*, 2013], one general circulation model study shows a decrease [*Rind et al.*, 1998] and others no significant trend [*Butchart et al.*, 2000; *SPARC CCMVal*, 2010; *Mitchell et al.*, 2012]. Possible causes for changes in SSW frequency under increased GHG conditions are found to be changes in the stratospheric meridional overturning circulation, which itself occurs due to a combination of changes in wave flux from the troposphere into the stratosphere [*Ayarzagüena et al.*, 2013; *Schimanke et al.*, 2013], and changes in middle atmospheric zonal winds [*McLandress and Shepherd*, 2009; *Schimanke et al.*, 2013].

There are still a number of open questions about the influence of natural and anthropogenic factors on the polar vortex and the frequency of SSWs. Nonlinear interactions between the single forcing factors complicate the gain of insight, e.g., because QBO east years tend to coincide with El Niño years. Since observational records of the stratosphere are short and it is complicated if not impossible to separate the influence of the respective factors, we designed sensitivity simulations with a high-top stratosphere-resolving chemistry-climate model (CCM) to systematically switch on and off the single factors and analyze their respective roles. We use National Center for Atmospheric Research (NCAR)'s Community Earth System Model (CESM) version 1.0.2, a state-of-the-art coupled model system with the Whole Atmosphere Community Climate Model (WACCM) version 4 as its atmospheric component.

Our paper extends the study of *Richter et al.* [2011], who analyzed the influence of the QBO and ENSO on SSW frequency in a set of 30 year model simulations. They found no significant change in the number of SSWs when they removed the QBO or variable SSTs from their simulations but a significant drop in the frequency when both factors were removed at once. We now investigate longer simulations (two 56 year and two 145 year simulations) and additionally consider the influence of anthropogenic forcings. In this study, we investigate not only the frequency of major warmings but also their life cycle, starting from its preconditioning in the troposphere to the warming event itself and the downward coupling to the troposphere afterward.

Several studies investigated the preconditioning of major SSWs and found a geographically dependent connection between different types of SSWs and tropospheric blockings [e.g., *Quiroz*, 1986; *Taguchi*, 2008; *Martius et al.*, 2009; *Woollings et al.*, 2010; *Castanheira and Barriopedro*, 2010; *Nishii et al.*, 2011; *Bancala et al.*, 2012]. Blockings are quasi-stationary and persistent anticyclonic systems with a strong meridional component that interrupts the zonal flow. *Nishii et al.* [2011] found that tropospheric blockings over the Euro-Atlantic sector tend to enhance upward planetary wave propagation and can lead to major warmings, while blockings over the western Pacific region tend to suppress planetary wave propagation and hence the development of SSWs. *Martius et al.* [2009] and *Castanheira and Barriopedro* [2010] distinguish between the influence of blockings on different types of SSW events: the vortex displacement events—where the vortex is shifted off the pole—which are often preceded by blockings in the Euro-Atlantic basin, and the vortex-splitting events—where the vortex breaks up into two subvortices of comparable size—which are more favorable after blockings in the Pacific. *Bancala et al.* [2012], on the other hand, distinguish between "wave number-1" and "wave number-2" events based on the dominant wave pattern responsible for initiating the warming. They found that blockings in the Euro-Atlantic mostly lead to the development of wave number-1 events, and blockings in the Pacific mostly precede wave number-2 SSWs.

The warming event itself can be characterized by several benchmarks like its type (wave number-1 or wave number-2 [*Yoden et al.*, 1999], "split" or "displacement"), its strength, and its duration [*de la Torre et al.*, 2012]. In this study, we investigate if and how natural and anthropogenic factors influence these characteristics of major warmings.

We also analyze possible differences in the surface response following a major warming. When the geopotential height anomaly propagates down to the troposphere after major warmings [*Quiroz*, 1977; *Kodera and Chiba*, 1995; *Baldwin and Dunkerton*, 2001; *Thompson et al.*, 2002; *Mitchell et al.*, 2013], the resulting surface pattern strongly projects onto the negative phase of the North Atlantic Oscillation (NAO) or the Arctic Oscillation (AO) [*Baldwin and Dunkerton*, 2001; *Charlton and Polvani*, 2007]. *Mitchell et al.* [2013] showed by analyzing reanalysis data that vortex split events lead to positive (negative) temperature anomalies over North America (Europe) while the surface response to vortex displacement events is much weaker. *Charlton and Polvani* [2007] found an additional surface anomaly to occur over the Pacific after SSW events which is reminiscent of the Pacific-North American pattern (PNA) [*Wallace and Gutzler*, 1981].

This paper is structured as follows: section 2 describes the CESM model and the CESM sensitivity experiments. Section 3 explains the major warming identification algorithm and the blocking index used in our analysis. In section 4, the SSW frequency as well as the climatological background state of the NH polar winter stratosphere are analyzed for the different sensitivity experiments. Section 5 then examines differences in the evolution of SSW events (preconditioning, mature and declining phase) for all simulations. Finally, the results are summarized and discussed in section 6.

2. Model Description, Experiments, and Reanalysis Data

The forcing experiments analyzed in this study were performed with the Community Earth System Model (CESM), developed at the National Center for Atmospheric Research (NCAR). CESM is a state-of-the-art coupled model system which is based upon the Community Climate System Model (CCSM4) [*Gent et al.*, 2011]. It includes an interactive ocean Parallel Ocean Program (POP), land Community Land Model (CLM), sea ice Community Ice CodE (CICE), and atmosphere (optionally WACCM or Community Atmosphere Model (CAM)) component [*Marsh et al.*, 2013]. For the simulations analyzed here, CESM was used in its version 1.0.2 with the Whole Atmosphere Community Climate Model (WACCM) version 4 as the atmospheric component, designated CESM1(WACCM) in *Marsh et al.* [2013]. WACCM is a fully interactive chemistry-climate model which has been used independently in many studies of middle to upper atmosphere dynamics and

Table 1. Summary of CESM Experiments

Name	Period	GHGs and ODSs	SSTs/Sea Ice	QBO
GHG	1955–2099 (145 years)	observations and RCP8.5 scenario	interactively	nudged
NATURAL	1955–2099 (145 years)	fixed at 1960s level	interactively	nudged
Fixed SSTs	1955–2010 (56 years)	fixed at 1960s level	climatological annual cycle from NATURAL	nudged
NOQBO	1955–2010 (56 years)	fixed at 1960s level	interactively	no

chemistry [e.g., *Taguchi and Hartmann*, 2006; *Matthes et al.*, 2010; *Garcia et al.*, 2011; *Smith et al.*, 2011; *Limpasuvan et al.*, 2012; *Matthes et al.*, 2013]. It extends from the Earth's surface to ~140 km altitude [*Garcia et al.*, 2007; *Richter et al.*, 2010] and is used here on a horizontal grid of $1.9 \times 2.5°$ (latitude × longitude) and on 66 vertical levels. Chemistry is calculated interactively in the chemistry module based on version 3 of the Model for OZone And Related chemical Tracers (MOZART) [*Kinnison et al.*, 2007]. The interactive ocean and sea ice components are run on a $1° \times 1°$ triangular horizontal grid and are described in *Holland et al.* [2012] and *Danabasoglu et al.* [2012]. Note that the amplitude of ENSO is overestimated compared to observations [*Marsh et al.*, 2013].

To study the influence of natural and anthropogenic factors on SSWs, four different simulations were performed where these factors were systematically switched on and off to allow the separation of the individual contributions. A summary of the experiments is given in Table 1. Due to the complexity of the model system and the fact that chemistry is calculated interactively in WACCM, the computational effort of CESM is extremely high so that only one run per experiment could be performed.

All factors considered in this study, namely, anthropogenic forcings, the QBO, and SSTs (including sea ice concentrations), were used for the 145 year CESM "GHG" experiment. GHGs and ODSs follow observations from 1955 to 2005, and the Coupled Model Intercomparison Project 5 (CMIP5) Representative Concentration Pathways (RCP) Scenario 8.5 thereafter until 2099 [*Meinshausen et al.*, 2011; *Taylor et al.*, 2012]. The QBO is nudged between 22°S and N as described in *Matthes et al.* [2010] and *Hansen et al.* [2013] and extended into the future by projecting Fourier coefficients of the oscillation. The solar cycle is prescribed as spectrally resolved daily variations following *Lean et al.* [2005]; for the 21st century, the last four solar cycles before 2005 are repeated. Of all the experiments which were performed, the GHG simulation is the one whose forcings are closest to observations in the twentieth century. This simulation is similar to the CESM1 (WACCM) RCP8.5 simulation submitted to CMIP5 by the NCAR CESM group [*Hurrell et al.*, 2013].

In the "NATURAL" experiment only natural and no anthropogenic forcings are considered. This is done by keeping GHGs and ODSs fixed at the 1960s level over the whole simulation period (1955–2099; for CO_2, e.g., this means an annual mean value of 316 ppmv). All other settings are equivalent to the GHG experiment.

The "Fixed SSTs" simulation uses the same forcings as the NATURAL experiment except that the underlying SSTs and sea ice for the 56 simulated years (1955–2010) were computed as the climatological monthly varying fields from the NATURAL experiment. As this simulation does not contain interannual variations in SSTs, the interannual memory of the ocean is switched off and it does not include oceanic phenomena such as ENSO or extratropical interdecadal and intradecadal Atlantic and Pacific variability. Of the factors investigated in this study, the only interannually varying forcing here is the QBO. Consequently, this experiment can be used to investigate the pure QBO effect without any influence of oceanic variability signals.

The 56 year "NOQBO" experiment (spanning the period 1955–2010 as in Fixed SSTs) uses again the same settings as the NATURAL simulation but without the QBO nudging. This leads to relatively constant weak easterlies of about −10 m/s in the equatorial stratosphere instead of the quasi-biennial oscillation between westerly and easterly winds in this region. Thus, the SSTs and sea ice are the only interannually varying forcing in this experiment which makes it well suited for analyzing pure SST and sea ice induced signals, especially those associated with ENSO.

This set of sensitivity experiments will be used in the following to systematically study the influence of natural and anthropogenic factors on SSWs. We compare the results of the sensitivity simulations to the European Centre for Medium-Range Weather Forecasts Re-Analyis (ERA) products ERA40 [*Uppala et al.*, 2004] and ERA-Interim [*Simmons et al.*, 2006], which have been combined into one data set as described in *Blume et al.* [2012], referred to as "ERA" hereafter. This combined data set resolves the stratosphere up to 1 hPa and spans the period from 1958 to 2012.

3. Methods

3.1. Identification of Stratospheric Sudden Warmings

According to the WMO definition, a major SSW occurs if the zonal mean temperature difference between 60°N and 90°N increases significantly in a couple of days and the zonal mean zonal wind at 60°, 10 hPa reverses from westerly to easterly [*Andrews et al.*, 1987; *Labitzke and Naujokat*, 2000]. Many studies which deal with different questions on SSWs consider the wind criterion only and neglect the temperature difference between 60°N and 90°N [e.g., *Charlton and Polvani*, 2007; *Garfinkel et al.*, 2012; *Schimanke et al.*, 2013]. Another approach is to use the first empirical orthogonal function (EOF) and its respective principal component (PC), e.g., of geopotential height anomalies (which then defines the Northern Annular Mode (NAM) [*Baldwin and Dunkerton*, 2001]) or of zonal mean zonal wind anomalies at 50 hPa (as done by *Limpasuvan et al.* [2004]) to define disturbed NH winter states.

Black and McDaniel [2004] analyzed potential vorticity in the context of stratospheric NAM events, and recently *Mitchell et al.* [2013] used the distribution of potential vorticity for the definition of weak vortex events.

We follow the original WMO definition of SSWs: a major warming is identified if between November and April (1) the zonal mean zonal wind at 60°N, 10 hPa is easterly and (2) the temperature difference between 60 and 90°N at 10 hPa is positive for at least 5 days within the period from 10 days before to 4 days after the day of the wind reversal, which is referred to hereafter as the central date of the warming (following WMO; *Labitzke and Naujokat* [2000]). No second warming can be defined within a period of 20 days after a major warming event, and all fluctuations around zero wind speed during this period are then counted as one event.

In this study, we will neglect minor warmings, which are disturbed states of the NH winter stratosphere with an anomalous increase in temperature but without a reversal of the circulation [*Labitzke and Naujokat*, 2000], and final warmings, which indicate the return to the summer circulation. We will focus only on major warmings, as they are the strongest manifestation of the dynamical coupling between the stratosphere and the troposphere.

Applying our identification algorithm to ERA leads to a total number of 26 major warmings in the period 1958–2002, i.e., three fewer than in *Charlton and Polvani* [2007] which is due to the additionally applied temperature criterion, and 31 major warmings in the period 1958–2012.

We used the method described in *Charlton et al.* [2007] to compute the statistical significance of the difference in major warming frequency between two different data sets with a two-sided *t* test. *Charlton et al.* [2007] argue that one can assume every winter to be an independent observation of the major warming frequency per winter. Then, an expected value and a standard error of the frequency can be computed, and two data sets can be compared with a two-sided *t* test.

3.2. Blockings

Several studies found a relation between the occurrence of SSWs and tropospheric blockings in the Euro-Atlantic and Pacific region [e.g., *Quiroz*, 1986; *Taguchi*, 2008; *Martius et al.*, 2009; *Woollings et al.*, 2010; *Castanheira and Barriopedro*, 2010; *Bancala et al.*, 2012]. We will test in this study whether this relationship holds in our model and how it depends on the different factors. We compute a daily blocking index following *Tibaldi and Molteni* [1990] which depends on the geopotential height fields at 500 hPa and compares midlatitudes (60°N) with higher (80°N) and lower (40°N) latitudes. According to this definition, a longitude is defined as being blocked if the geopotential height gradient between midlatitudes and lower latitudes is positive and the gradient between high latitudes and midlatitudes falls below −10 m per degree. This has to be fulfilled over at least three adjacent longitudes (i.e., 5° for our longitudinal resolution of 2.5°) and for at least 5 days.

4. Stratospheric Sudden Warming Frequency

In this section the seasonal distribution of major warmings over NH winter months is presented for the different experiments. Afterward, we address differences in the major warming distributions by examining differences in the climatological background winds, waves, and wave-mean flow interaction.

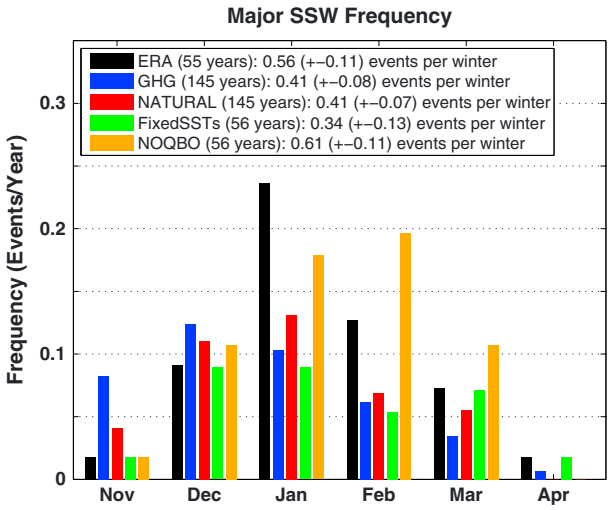

Figure 1. Frequency of major warmings in NH winter months in ERA and CESM sensitivity simulations. Numbers in brackets indicate the standard error of the SSW total winter frequency.

4.1. SSW Seasonal Distribution

Figure 1 shows the seasonal distribution (November through April) of major warmings for ERA and our four CESM sensitivity experiments in relative frequency of warming events per month and year. The observed SSW distribution (ERA, black bars) is well known: the frequency of major warmings increases steadily from November until its maximum of 0.23 events per year in January and decreases steadily afterward until the end of the winter. The average frequency of major warmings for the period 1958–2012 obtained for ERA with our selection algorithm is 0.56 events per year.

For the GHG experiment, we analyzed the 20th and 21st centuries separately (not shown) to detect potential differences in major warming frequency that might occur due to the strong GHG forcing (the RCP8.5 scenario). We neither found an increase in the number of major warmings until the end of the 21st century as was reported, e.g., in *Huebener et al.* [2007], *Charlton-Perez et al.* [2008], *Bell et al.* [2009], *Schimanke et al.* [2013], and *Ayarzagüena et al.* [2013], nor a decrease as found by *Rind et al.* [1998], so our results are in line with *Butchart et al.* [2000]; *SPARC CCMVal* [2010] and *Mitchell et al.* [2012]. Therefore, we will not distinguish between the two centuries in the following analysis but analyze the entire period from 1955 to 2099.

No large differences in SSW frequency are seen between ERA and the CESM sensitivity experiments in early winter (November and December), with the exception of the GHG experiment (blue bars) showing a higher major warming frequency in November. During January and February, all simulations show a lower major warming frequency than ERA, except the NOQBO experiment (orange bars), which shows a higher SSW frequency than ERA in February and a notably higher frequency than the other three runs in both months. This endures until March, although the differences become smaller.

Over the whole winter season, we find the highest SSW frequency in the NOQBO experiment, where 0.61 events per winter occur during the simulation period (1955–2010). The fewest SSWs occur in the Fixed SSTs run (green bars; 0.34 events per year between 1955 and 2010) where the seasonal distribution is very flat. The applied *t* test reveals that the differences between the major warming frequencies in NOQBO and Fixed SSTs are statistically significant at the 95% confidence interval and between the major warming frequencies in NOQBO and both GHG and NATURAL at the 90% confidence interval. That means that in our simulations variable SSTs and the QBO influence the number of SSWs significantly, while anthropogenic GHGs and ODSs do not have a measurable effect. A summary of the number and frequency of major warmings in ERA and the CESM sensitivity experiments can be found in the second and third columns in Table 2.

Table 2. Summary of SSW Characteristics in ERA and CESM Forcing Experiments[a]

Name	SSWs	SSW Frequency	Blocking ATL/PAC/Both	Prewarming W1/W2/W3	Duration (Days) Mean (Max/Min)	Amplitude (°C) Mean (Max/Min)	Displace/Split
ERA	31 (55 years)	0.56	11 / 3 / 11	24 / 7 / 0	8.0 (30 / 1)	13.6 (28.4 / −2.1)	18 / 13
GHG	60 (145 years)	0.41	17 / 4 / 3	57 / 3 / 0	6.1 (27 / 1)	13.8 (28.2 / 3.3)	55 / 5
NATURAL	60 (145 years)	0.41	13 / 6 / 5	57 / 1 / 2	6.8 (26 / 1)	13.8 (24.5 / −2.4)	56 / 4
Fixed SSTs	19 (56 years)	0.34	5 / 3 / 3	17 / 2 / 0	6.5 (25 / 1)	14.6 (23.1 / 7.8)	15 / 4
NOQBO	35 (56 years)	0.61	6 / 4 / 4	35 / 0 / 0	6.9 (22 / 1)	14.2 (22.7 / 1.8)	30 / 5

[a]In the fourth column, the three numbers indicate how many of the total number of SSWs (see first column) are preceded by a blocking in either the Atlantic or the Pacific or in both of the regions. The fifth column divides the total number of SSWs in wave numbers 1, 2, and 3 SSWs, and the eighth column in displace and split SSWs. See text for further details.

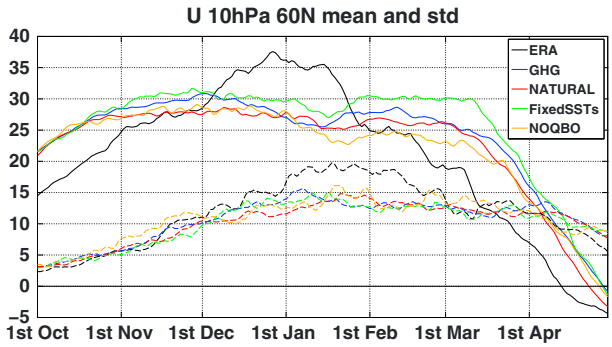

Figure 2. Development of the long-term mean (solid lines) and interannual standard deviation (dashed lines) of daily zonal mean zonal wind at 60°N, 10 hPa for ERA and CESM sensitivity simulations.

Our result that removing one factor, the QBO or variable SSTs, significantly changes (increases or decreases, respectively) the SSW frequency is different from the results of *Richter et al.* [2011] who only found a significant decrease (and a significant impact on the climatological background state) when both QBO and SST variability were removed. However, our simulations are almost twice as long and therefore provide better statistics for the detection of variability beyond the internal variability of the polar vortex.

In our simulation, we find clusters of major SSWs throughout the different simulations which are similar to observations (not shown). In GHG, NATURAL, and Fixed SSTs, there are two to three periods of about 10 years without any major SSWs, and in all simulations there is at least one decade with eight or nine major SSWs. However, the time series are too short for a detailed analysis of low-frequency fluctuations of major SSW occurrence.

4.2. Climatological NH Winter Conditions

SSWs are prominent examples of wave-mean flow interaction. Therefore, the differences in the major warming frequency between the different sensitivity experiments may arise from either (a) differences in the climatological stratospheric polar night jet (PNJ) (which is influenced by the natural and anthropogenic factors), (b) differences in planetary wave generation and/or propagation, (c) differences in the interaction between these waves with the mean flow, or from a combination of all. This will be investigated in the following section.

4.2.1. PNJ Strength and Variability

Shown in Figure 2 is the development of the daily zonal mean zonal wind at 60°N, 10 hPa, showing the average (solid lines) and the interannual standard deviation (dashed lines) over all winters for ERA and the CESM sensitivity experiments. The PNJ strength and evolution differ remarkably between ERA and the CESM simulations: while in ERA the wind increases until the end of December to a maximum of about 37 m/s, it stays almost constantly around 30 m/s from November on in CESM.

The zonal mean zonal wind develops similarly in the CESM experiments until the middle of January. Then two "extreme" cases develop: the highest PNJ wind speeds are found in the Fixed SSTs experiment and the lowest wind speeds in the NOQBO experiment, with differences of up to about 6–8 m/s in February and March. These two experiments also have statistically significant differences between the major warming frequency (see previous section), which are most prominent in January through March and therefore consistent with the findings here. The GHG and NATURAL experiments show PNJ strengths that lie between the two extreme cases.

Our knowledge about the dynamics between the equatorial QBO and the polar stratosphere implies a comparably weaker, and hence more easily disturbed, vortex in the NOQBO simulation, because the equatorial stratospheric winds in this experiment resemble a permanent easterly phase of the QBO. The effect of removing the QBO westerly phase is strongest from the end of December until the middle of March, which is consistent with the influence on major warming frequency which is also strongest in these months.

In the Fixed SSTs run, in contrast, the vortex is stronger and therefore less easily disturbed, probably because this simulation lacks El Niño events, which have been shown to significantly weaken the stratospheric polar vortex due to enhanced tropospheric wave forcing [*Van Loon and Labitzke*, 1987].

In our GHG simulation, a weakening of the stratospheric PNJ occurs poleward and upward of 60°N, 10 hPa, until the end of the 21st century due to increasing anthropogenic GHGs, together with a strengthening

(and shift) of the tropospheric subtropical jet (not shown), which is a robust outcome of tropospheric warming and stratospheric cooling under increased GHGs [see, e.g., *Shepherd and Mclandress*, 2011]. The region around 60°N, 10 hPa, which is shown in Figure 2 and where the wind criterion for the major warming definition is applied, lies exactly in the transition between these two opposed signals, so that no trend is seen here. Therefore, it is consistent to see no change in SSW frequency due to increasing anthropogenic GHGs in our study.

From the middle of April on, the PNJ strength again evolves very similarly in the CESM experiments, though a remarkably large difference of about half a month exists in the vortex breakup day, i.e., the return to summer circulation, between ERA (13 April) and CESM (23 to 28 April).

The interannual variability, shown as interannual standard deviation in dashed lines in Figure 2, is higher in ERA than in the CESM simulations throughout January and February. This is consistent with the finding of a higher major warming frequency in ERA, especially in January, but the differences in standard deviation between ERA and CESM become smaller in PNJ regions closer to the pole. However, no remarkable differences are seen between the simulations.

4.2.2. Wave Generation

Besides an impact on the PNJ strength and variability, the different factors might have an impact on the generation of waves in the troposphere, which could then lead to differences in the propagation of these waves into the stratosphere and the PNJ region and hence have an effect on SSWs. To analyze a possible influence on wave generation, we investigate the amplitudes of the geopotential height (GPH) waves in the troposphere and distinguish between planetary (wave numbers 1–3) and smaller-scale (wave numbers >3) waves. Figure 3 shows the amplitude of these waves for the NATURAL simulation (first row) averaged over December and January, i.e., up to 1 month before the largest differences between the CESM sensitivity simulations in major warming frequency occur (see Figure 1). The second to fourth rows in Figure 3 show differences in wave amplitudes between the GHG, the Fixed SSTs, and the NOQBO simulation with respect to the NATURAL simulation.

The amplitudes of planetary waves (left column) are significantly reduced in the Fixed SSTs experiment poleward of around 40°N throughout the middle to upper troposphere and lower stratosphere. This is according to our expectations, since planetary waves are, e.g., generated due to SST variabilities which are reduced in this experiment. The NOQBO simulation shows a similar response as the Fixed SSTs run in midlatitudes, though the negative signal is less statistically significant. Increasing GHGs lead to an upward shift of the wave amplitude maximum with a significant reduction of planetary wave amplitudes in the troposphere but a significant increase in the upper troposphere and lower stratosphere.

The strongest influence on smaller-scale waves (right column in Figure 3) is seen in the GHG experiment, where a significant amplitude increase centered around 50°N, 200 hPa occurs. The responses in both the Fixed SSTs and the NOQBO experiments are smaller compared to the GHG simulation and confined to the middle troposphere.

In summary, the effects of fixing the SSTs and switching off the QBO on wave generation are similar. Differences between both experiments which occur in the stratosphere might therefore be dominated by differences in the background winds and therefore wave propagation and wave-mean flow interactions. This will be further investigated in the following section.

4.2.3. Wave Propagation and Wave-Mean Flow Interaction

To analyze the strength and propagation direction of planetary waves, we use the Eliassen-Palm (EP) flux vector which is described in the Transformed Eulerian Mean (TEM) framework [*Andrews et al.*, 1987]. The divergence of the EP flux vector describes the interaction of resolved waves with the mean flow: in a region of EP flux divergence (convergence), the mean flow is accelerated to the east (west), e.g., prevailing westerly winds are accelerated (decelerated).

We compare the PNJ strength (represented by the zonal mean zonal wind), the EP flux vector, and its divergence averaged over January-February (JF), as the influence of the different factors on SSW frequency was found to be largest in these months. Figure 4a shows these three parameters for the NATURAL simulation. To highlight differences due to the different factors, Figures 4b–4d show these parameters for the GHG, the Fixed SSTs, and the NOQBO simulations as differences with respect to the NATURAL experiment. In JF, upward propagation of planetary waves from the troposphere into the stratospheric PNJ region occurs

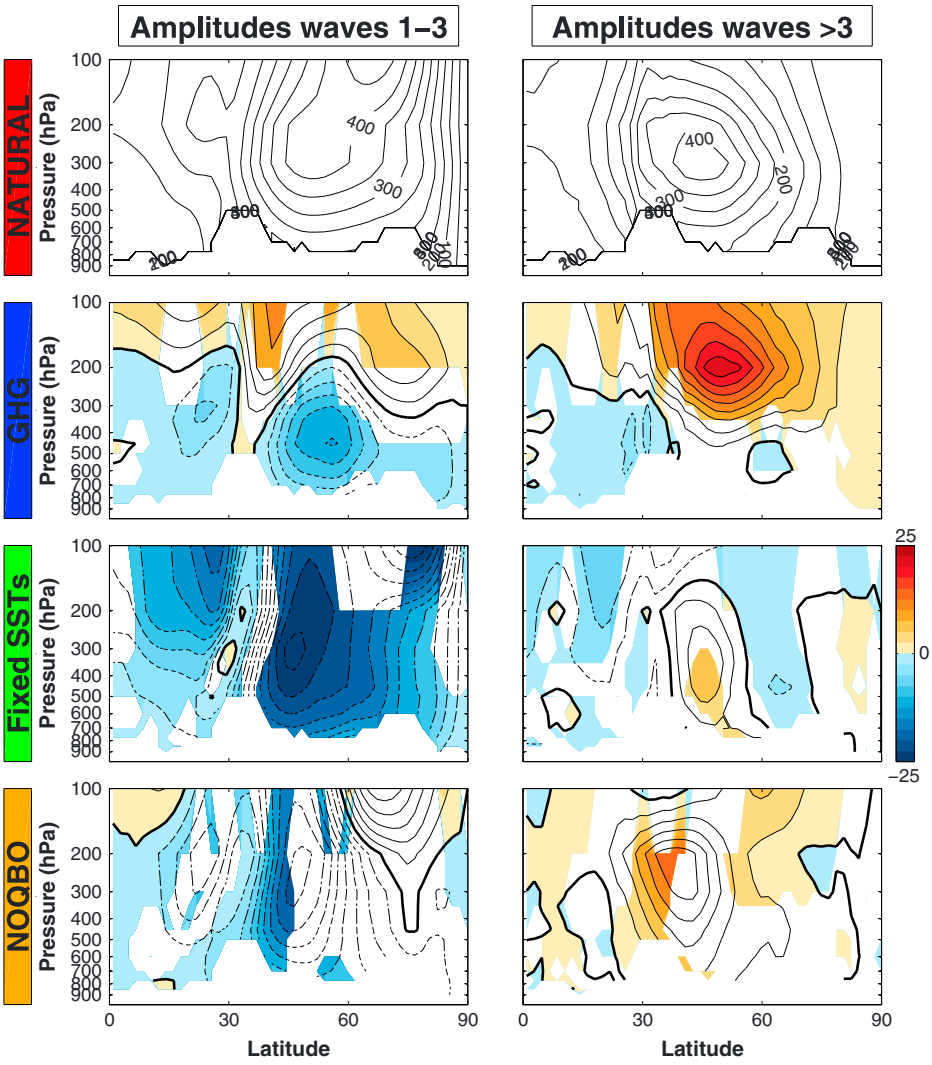

Figure 3. (first row) GPH wave amplitudes (contour interval: 50 m) in the NATURAL simulation; (left) planetary-scale waves (wave numbers 1–3), (right) smaller-scale waves (wave numbers >3). (second to fourth rows) Differences of planetary and smaller-scale wave amplitudes (contour interval: 2.5 m) between (second row) the GHG, (third row) the Fixed SSTs, (fourth row) the NOQBO simulation, and the NATURAL simulation, respectively, for the mean over December and January; shading indicates 95% statistical significance.

poleward of 50°N (Figure 4a). A large EP flux convergence region around 300 hPa poleward of 40°N indicates a deceleration of prevailing westerlies by wave-mean flow interactions.

As seen before in Figure 2, the PNJ strength (indicated by black contours in Figure 4) only shows very small differences between the GHG and the NATURAL experiments (Figure 4b), while larger differences are seen throughout the vortex region for the Fixed SSTs and NOQBO experiments (black contours in Figures 4c and 4d, respectively). In addition to the stronger PNJ, a downward and equatorward anomaly of the EP flux vector occurs between 40 and 60°N along the tropopause in the Fixed SSTs run, together with a downward anomaly in the lower to middle stratosphere northward of 70°N and a divergence anomaly in the lower PNJ region. Together with the significantly reduced planetary wave generation seen before (Figure 3), this suggests a weaker planetary wave propagation into the region of the stratospheric polar vortex and weaker deceleration of the westerlies in the lower polar stratosphere. This creates conditions which allow a stable, strong, and cold polar vortex and hence, as found before, a relatively lower number of major warmings when SSTs are kept fixed.

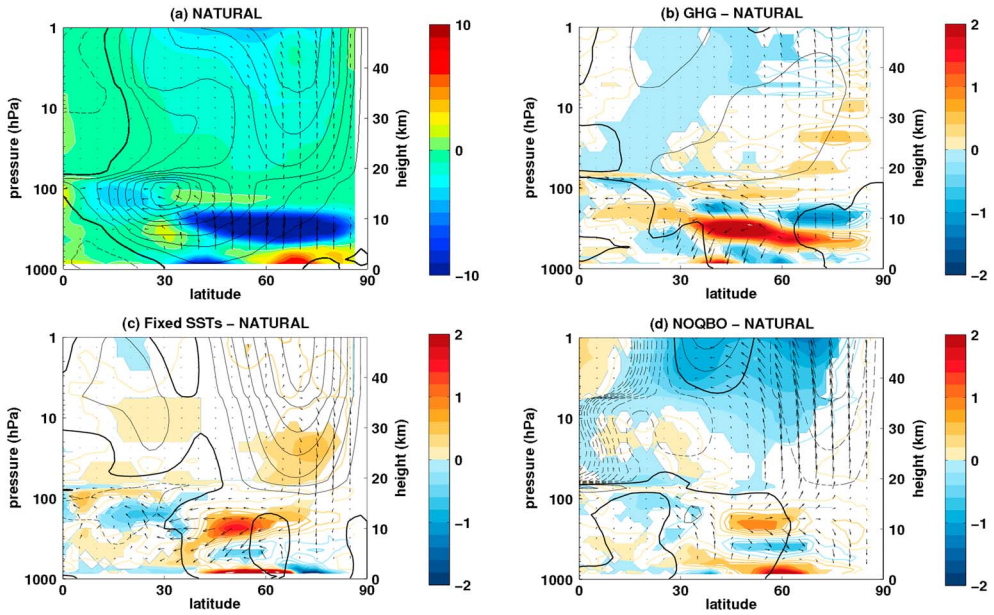

Figure 4. (a) January-February climatological zonal mean zonal wind (contours; contour interval 5 m/s, dashed lines indicate easterly winds, bold black line is the zero wind line), EP flux vector (arrows; scaled with the square root of pressure), and its divergence (colors; in $ms^{-1}d^{-1}$, positive values indicate divergence, white line is the zero line) for the NATURAL simulation. Differences of the zonal mean zonal wind (black contours; contour interval 1 m/s, dashed lines indicate easterly winds, bold line is the zero wind line), EP flux vector (arrows; scaled with the square root of pressure), and its divergence (colored contours and color shading; in $ms^{-1}d^{-1}$, shading indicates 95% statistical significance) between (b) the GHG and the NATURAL simulation, (c) the Fixed SSTs and the NATURAL simulation, and (d) the NOQBO simulation and the NATURAL simulation for January-February.

In contrast, in addition to the weakened PNJ in the NOQBO compared to the NATURAL experiment, the poleward and upward propagation of planetary waves into the polar vortex region is enhanced northward of 50°N above 200 hPa throughout the stratosphere. Together with enhanced convergence (and therefore PNJ deceleration) on the equatorward flank of the polar vortex, all this results in a weak, more disturbed and warmer vortex and is therefore consistent with the previous finding of an increased major warming frequency in this simulation.

The GHG experiment shows the largest changes of all simulations in EP flux divergence in the mid-latitude to high-latitude troposphere. These changes might result from the statistically significant changes in smaller-scale wave amplitudes in these regions, which are considerably smaller in the other experiments (Figure 3).

In summary, the differences in SSW frequency can be explained by differences in PNJ strength, resulting mainly from differences in wave propagation and wave-mean flow interaction and less from differences in wave generation: fewest SSWs occur without SST variability, where we find the strongest PNJ and reduced wave (generation and) propagation into the vortex region, and most SSWs occur without QBO nudging, where the PNJ is weakest of all experiments and where wave propagation into the PNJ region is enhanced. The interannual variability in PNJ strength is not changed significantly by the respective factors.

5. Major Warming Life Cycles

In the previous section we have compared the occurrence frequency of SSWs for different forcing factors and saw that removing SST and QBO variability has the largest effect on the number of SSWs, because it has the strongest influence on the polar stratospheric basic state due to changes in planetary wave propagation and in the mean flow. Here we will focus on the warming event itself to examine whether and how the different factors affect the life cycle of SSWs. We will start with the preconditioning phase, then investigate the phase around the central date, and finally study the coupling to the troposphere afterward.

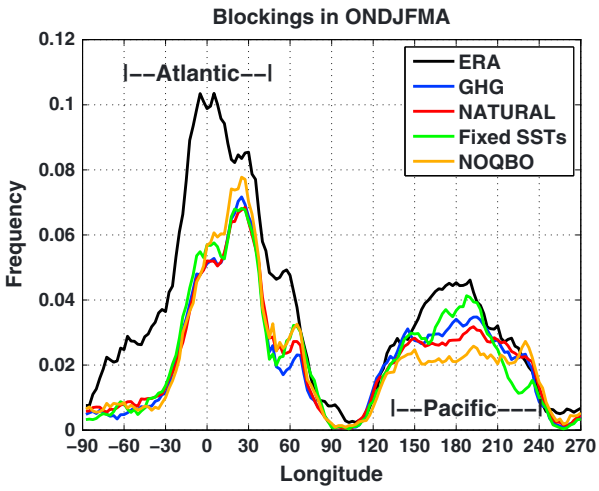

Figure 5. Frequency of days with tropospheric blocking between October and April at each longitude, for ERA and CESM sensitivity simulations. See text for details.

5.1. Preconditioning

Figure 5 shows the frequency of days with a tropospheric blocking in the NH extended winter season (October through April) over longitude, comparing ERA and the four CESM sensitivity experiments. Two frequency maxima can be detected in all data sets: one in the Euro-Atlantic (60°W–45°E) and a second one in the Pacific (135°E–120°W). Both maxima are remarkably reduced in CESM by about 20%, and the maximum in the Atlantic is shifted eastward by about 30°. An underestimation of blockings in climate models is a common model bias and well documented, e.g., in *Scaife et al.* [2010] and *Anstey et al.* [2013]. For CESM, the reduced frequency of blocking occurrence seen over the whole extended winter season has been shown in *Marsh et al.* [2013]. Blocking is reduced in all months but particularly in December and January (not shown) which is congruent with the reduced SSW frequency in these months (Figure 1). For the Pacific, the blocking frequency is too low for all months.

In GHG, NATURAL, and NOQBO, 40% of all SSWs are preceded by a blocking in at least one of the two regions, which is mainly the Euro-Atlantic area (see Table 2, fourth column). Comparing all CESM experiments, most blockings in the context of SSWs occur in the Fixed SSTs experiment where in 58% of all cases SSWs are preceded by at least one blocking and 16% by a blocking in both the Atlantic and Pacific regions. However, this is still less than in ERA, where around 80% of all SSWs are preceded by at least one blocking. The occurrence thereby refers to the period of up to 10 days prior to the central date. If we consider a period of 20 days before the major warming, around 55% (78%) of all events are preceded by at least one blocking in GHG, NATURAL, and NOQBO (Fixed SSTs). Because the number of major warmings preceded or not preceded by blocking is about the same, we cannot detect a general statistical relationship between the occurrence of blockings and SSWs.

Bancala et al. [2012] showed, for observational and model data, that blockings in the Euro-Atlantic are related to wave number-1 major warmings and blockings in the Pacific to wave number-2 major warmings. To investigate that for our CESM sensitivity experiments, we classified all major warmings as wave number-1 (W1), 2 (W2), or 3 (W3) events. This is done by comparing the amplitudes of geopotential height waves 1, 2, and 3 at 60°N at 10 and 50 hPa as well as the waves 1 and 2 components of the heatflux at 60°N, 100 hPa, computed as described by *Pawson and Kubitz* [1996], during the phase of strongest intensification. While in ERA about 25% of all major warmings are W2 events (and the remaining 75% are W1 events), we find only very few W2 events in our CESM experiments: three (of 60 events) in GHG, one in NATURAL, and two in the Fixed SSTs simulation (Table 2, fifth column). This may be related to the reduced frequency of tropospheric blockings discussed above, since especially blockings in the Pacific have been mentioned to be able to induce W2 events [*Martius et al.*, 2009; *Castanheira and Barriopedro*, 2010; *Bancala et al.*, 2012]. In our simulations, three of the six W2 events are preceded by a blocking in at least one of the two regions, Euro-Atlantic or Pacific. Interestingly, two W3 events occur in the NATURAL experiment which, at least to our knowledge, has not been reported before. These events are very weak in terms of easterly winds and temperature anomaly at the central date. However, these W3 events could also be a model artifact and need further investigation.

To further investigate the planetary wave behavior prior to the central date, we computed composites of daily anomalies of heat flux wave components 1 and 2 at 60°N, 100 hPa, over all SSWs following *Pawson and Kubitz* [1996], as well as daily anomalies of GPH wave 1 and 2 amplitudes at 60°N, 10 hPa. This is shown in Figure 6 for the period of 40 days prior to the SSW to 40 days after. For ERA, we see an increase in both the

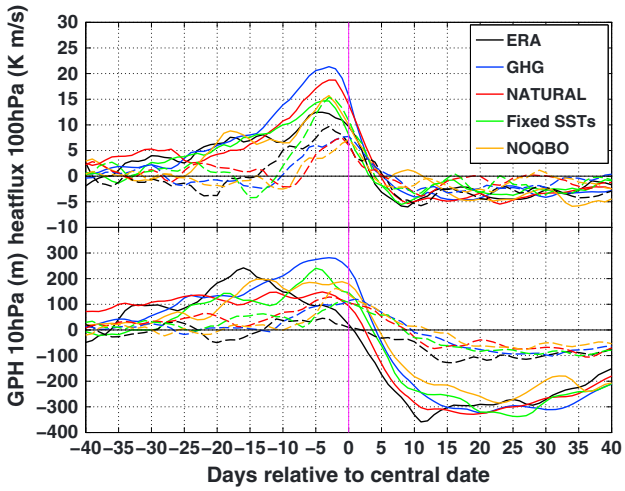

Figure 6. Composite of (top) heatflux anomalies at 60°N, 100 hPa (in K m/s) and (bottom) GPH wave anomalies at 60°N, 10 hPa (in m), wave 1 (solid lines) and wave 2 component (dashed lines) during major SSWs, for ERA and CESM sensitivity simulations.

heatflux wave 1 and wave 2 components before the major warming, with a maximum around 5 to 3 days before the central date. The GPH wave 1 at 10 hPa shows a maximum around 17 days before the central date. The figure reveals some similarities and differences between ERA and CESM and between the forcing experiments: all simulations show a peak in the heatflux wave 1 component around 3 days before the central date which is slightly overestimated but otherwise comparable to the observed peak in ERA. However, only in the Fixed SSTs simulation, the heatflux wave 1 and wave 2 components are about the same magnitude (solid and dashed green lines, upper part), whereas in the other CESM sensitivity experiments, the wave 1 component clearly dominates. In the NATURAL experiment, major warmings are preceded by an anomalous increase of heatflux and GPH wave 1 (red solid lines) which starts more than 5 weeks before the warming. Although the anomalies in the heatflux wave 1 component increase from 15 days before the warming on, the GPH wave 1 anomalies do not increase any further. This indicates a strong wave forcing from the troposphere which does not reach the 10 hPa level, which is shown in Figure 6, but propagates only up to around 30 hPa (not shown). This is especially different from the GHG experiment where the largest anomalies of all simulations occur in both heatflux and GPH wave 1 components (blue solid lines) from around 12 days before the warming on, suggesting that the tropospheric wave forcing prior to major warmings induces wave 1 propagation up to higher levels.

In the previous section we have seen a strong influence on the SSW frequency by the SST variability and the QBO; in this section we found that for the GPH planetary wave behavior during the preconditioning phase of major warmings, anthropogenic GHGs and ODSs play an important role by influencing the propagation and stratospheric influence of the tropospheric wave 1 forcing.

5.2. Around the Central Date

To examine some characteristics of major warmings around the central date, we first analyze the development of zonal wind and temperature in the vortex region. For this we computed composites over all SSWs of height-time sections of zonal mean zonal wind at 60°N and anomalies of polar cap (60–90°N) zonal mean temperature, shown in Figure 7. Values which are statistically significant at the 95% level are color shaded. Following *de la Torre et al.* [2012] or *Kolstad and Charlton-Perez* [2011], statistical significance of the composites is checked via a Monte Carlo method, where the "real" composite is tested against a 1000-member ensemble of random composites, each containing the same number of elements as the real composite and taking into account the months of the SSWs.

Directly around the central date, we see easterly winds in ERA and all simulations (left column in Figure 7), one criterion to define the major warmings. While these easterlies extend roughly between 15 and 0.02 hPa in the GHG, Fixed SSTs, and NOQBO experiment, they are bounded between 15 and 0.2 hPa in NATURAL, i.e., the easterlies do not reach as high as in the other experiments. The strongest easterlies which fall below −20 m/s can be found in the GHG experiment.

Already 5 weeks before the central date, statistically significant strong westerlies in the upper stratosphere precede the upcoming warming event in the NATURAL simulation. These wind anomalies are accompanied by positive anomalies of zonal mean polar cap temperature (right column in Figure 7) which are also statistically significant from 35 days before the major warming on and show a distinct maximum around 3 hPa at 25 days before the central date. This anomaly maximum in the prewarming phase was already described in the previous section as a maximum in wave activity starting 35 days before the central date. We find that this

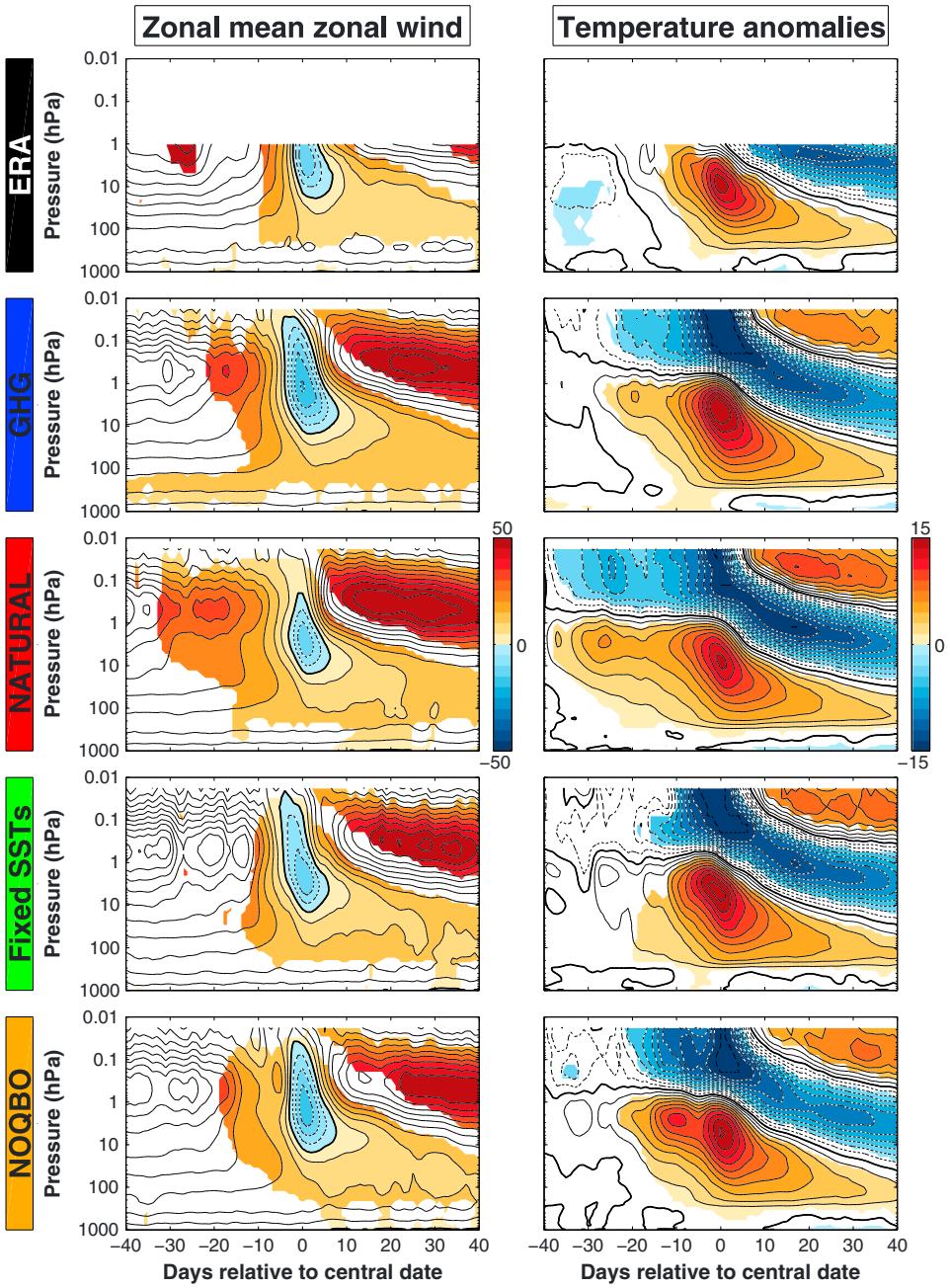

Figure 7. Height-time sections of (left column) zonal mean zonal wind at 60°N (contour interval: 5 m/s) and (right column) polar cap temperature anomalies (contour interval: 1.5°C) around central date; composite over all major SSWs; for ERA and CESM sensitivity experiments. Colors denote 95% statistical significance.

maximum is not due to the multiple occurrence of two SSWs at intervals of 25 days in a winter. Instead, we see that in several cases in NATURAL the zonal wind reverses in the upper stratosphere around 30–20 days before the central date of a warming which involves the warming anomaly seen at these lead times. As the wind reversal does not reach down to 10 hPa, no major but a minor SSW is defined in these cases. In the NOQBO simulation a "prewarming" seems to occur around 10 days before the major warming, which is seen as a maximum in positive temperature anomalies around 2 hPa. No comparable, statistically significant prewarming occurs in the Fixed SSTs simulation and in ERA, where the onset of the warmings occurs quite abruptly.

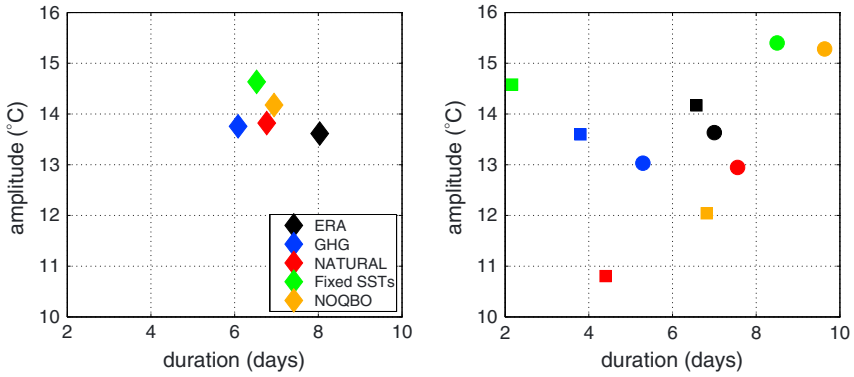

Figure 8. (left) Average amplitude and duration of all SSWs; (right) average amplitude and duration of SSWs preceded by an Atlantic (circles) or a Pacific (squares) blocking; in ERA and CESM sensitivity experiments.

After the central date, the warming anomaly propagates downward and then slowly fades out around 100 hPa in ERA and the CESM sensitivity runs. The downward propagation and surface impact after the warming will be further investigated in the next section.

To give another measure for the SSWs in the different CESM experiments, we calculated the duration and the amplitude of all events similar to *de la Torre et al.* [2012]. The duration of a SSW is defined as the number of consecutive days with easterlies at 60°N, 10 hPa; the amplitude is computed as the mean polar cap (60–90°N) temperature anomaly at 10 hPa within ±2 days around the central date. The average duration and amplitude of major warmings for the sensitivity experiments are shown in the left part of Figure 8 and listed in Table 2 in the sixth and seventh columns, with the numbers in brackets denoting the minimum and maximum values. For both duration and amplitude the differences are not statistically significant between any experiments or ERA, as tested with a two-sided *t* test. We also investigated if there are any differences in duration or amplitude between events that are preceded by Euro-Atlantic or Pacific blockings (see previous section) and found that SSWs which follow a Euro-Atlantic blocking are generally (in all simulations and ERA) longer than those preceded by a Pacific blocking (Figure 8, right part).

To distinguish between vortex split and displacement events, a distinction which refers to the wave number directly around the central date, we did a subjective analysis (like in *de la Torre et al.* [2012]) of the GPH fields at 10 hPa around the central date of the major warmings. The number of vortex split and displacement events is given in Table 2 in the eighth column. We found a few split SSWs in the CESM simulations, but compared to ERA, where more than 40% of all SSWs are classified as these events, their number is highly underestimated in CESM. This makes it difficult to do any further analysis with the distinction between displacement and split events or to draw any conclusions on this point. For the duration and amplitude of displacement and (the very few) split events, we did not find any significant differences.

5.3. After the Major Warming: Surface Impact

Strong major warmings have been shown to couple down from the stratosphere to the troposphere and have a significant influence on the surface circulation [e.g., *Baldwin and Dunkerton*, 2001; *Mitchell et al.*, 2013]. The most common method to investigate stratosphere-troposphere coupling is to analyze indices of the Northern and Southern Annular Modes (NAM and SAM) [*Baldwin and Dunkerton*, 2001]. We also use the NAM index to see whether any differences in the downward coupling occur in our CESM sensitivity experiments.

The NAM index is computed as the principal component (PC) of the first empirical orthogonal function (EOF) of daily, year-round GPH fields between 20 and 90°N. As suggested by *Baldwin and Thompson* [2009], we calculate the EOFs and PCs separately for each pressure level from zonal mean GPH anomalies. A positive (negative) NAM index implies an enhancement (diminishment) of the typical NAM pattern, corresponding with negative (positive) anomalies of GPH in the polar regions and positive (negative) anomalies in midlatitudes.

In Figure 9, composites of the time-height development of the NAM index are shown for all SSWs in ERA and all CESM experiments. During major warmings, the NAM index is negative (red colors in Figure 9) at almost

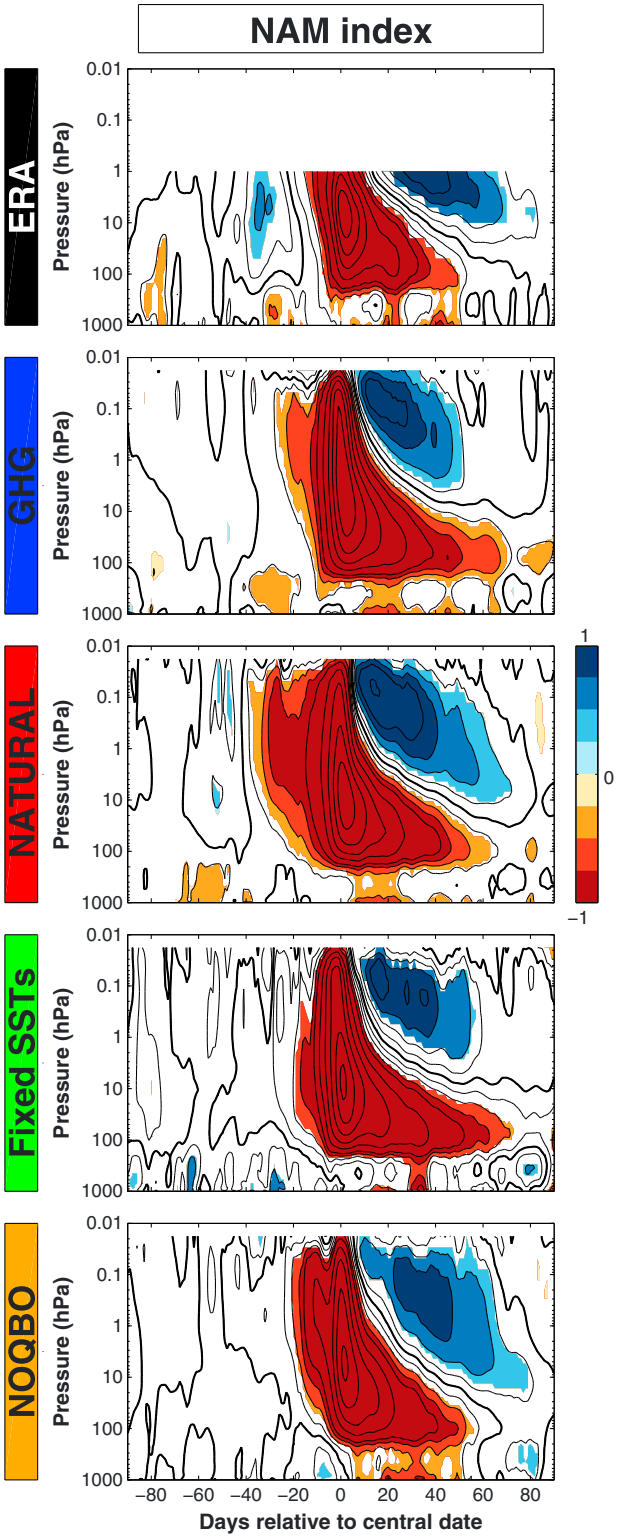

Figure 9. Height-time sections of NAM index around central date; contour interval 0.25 standard deviations for values between −1 and 1, 0.5 standard deviations for values below −1 and above 1; red (blue) colors denote 95% statistically significant negative (positive) values; composite over all major SSWs; for ERA and CESM sensitivity experiments.

all heights, with a minimum at the central date. In all simulations and in ERA we see a coupling to the troposphere indicated by the "dripping paint"-like negative NAM index in different periods after the central date. In ERA, the two most pronounced periods of coupling to the troposphere occur around 20 and 40 days after the central date, accompanied by an almost continuous statistically significant surface signal. In the GHG experiment, a significant influence on the surface occurs almost continuously between 7 and 50 days after the central date. The NATURAL simulation shows a similar behavior, especially in the significant downward coupling and surface imprint signals in the period 1–4 weeks after the central date. A very persistent statistically significant coupling of about 50 days to the troposphere and impact on the surface occurs in the NOQBO run. In contrast to the other experiments and ERA, only one short remarkable period of coupling to the troposphere can be found in the Fixed SSTs simulation, namely, after day 30, lasting about a week. This suggests that varying SSTs are needed to transport the signal of major warmings from the stratosphere to the troposphere.

In a last step, we examine the resulting surface impact pattern in the different simulations in more detail. For this we compute composites of all major warmings for sea level pressure (SLP) anomalies as 10 day averages in the periods before and after the central date of the warming. In Figure 10 these composites are shown exemplarily for the periods 20–10 days before, 5 days before to 5 days after, and 10–20 days after the major warming. In ERA and in the CESM sensitivity experiments the SLP anomalies before the central date resemble the positive phase of the Pacific-North American pattern (PNA) [*Wallace and Gutzler*, 1981], which was also described by *Charlton and Polvani* [2007]. Additionally, a positive SLP anomaly occurs above the Eurasian continent; however, not all

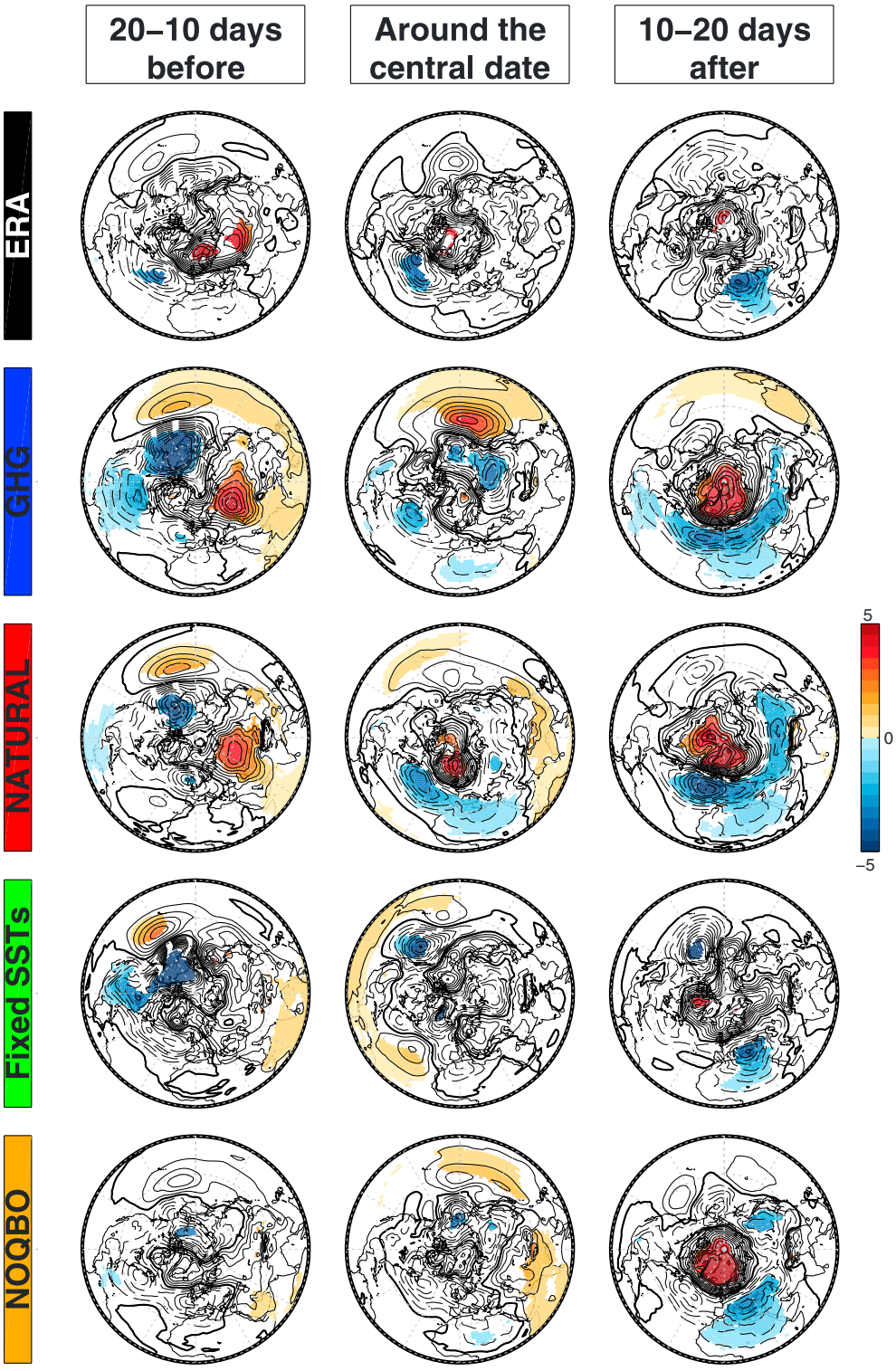

Figure 10. Composite of sea level pressure anomalies (in 0.5 hPa intervals), averaged over (from left to right) 20–10 days before, 5 days before to 5 days after, and 10–20 days after the central date, for ERA and CESM sensitivity simulations. Colors denote 95% statistical significance.

these signals are statistically significant in all simulations. The positive SLP anomaly above the Pacific persists through the central date and is still visible after the major warming in the GHG simulation.

Around and after the central date, the statistically significant SLP anomaly signals in ERA resemble a negative NAO pattern. The negative anomalies in the midlatitudes move from the central North Atlantic to the Mediterranean after the central date. In the GHG, NATURAL, and NOQBO simulation, the positive polar SLP anomaly is surrounded by a circular negative anomaly after the central date, making the signal resemble a negative AO (the "surface NAM") [*Thompson and Wallace*, 1998] pattern. However, the regions with statistically significant anomalies can mainly be found in the lower to midlatitudes between 30°W and 120°E, i.e., over the North Atlantic, Europe, North Africa and the Asian continent.

As found before for the coupling to the troposphere shown with the NAM index, only small differences occur between the GHG and the NATURAL simulation in the SLP surface response after the central date. In the NOQBO simulations, the negative AO pattern following major warmings has its maximum around 20–30 days after the central date (not shown), i.e., 10 days later than in the other simulations. In the Fixed SSTs experiment, the surface influence of major warmings does not only occur over a shorter period of time as seen before but potentially also over a smaller region, with the negative anomalies in the midlatitudes reduced to south Europe and north Africa. However, the latter finding might also be misinterpreted from a signal where the statistical significance is lower than in the other signals because of the small number of major warmings in the Fixed SSTs experiment. It therefore has to be confirmed, e.g., in longer simulations, if the ocean is really, as it seems here, influencing the stratosphere-troposphere coupling after major warmings and the persistence of the warmings's surface signal.

The surface impact of the major warmings can also be seen in anomalous SST signals both in the Atlantic and in the Pacific region (not shown) and is preserved longer in the CESM experiments with interactive ocean. According to *Barsugli and Battisti* [1998], this could be explained with the internal damping of anomalies due to surface heat fluxes which is enhanced when ocean and atmosphere are not coupled interactively, as in the Fixed SSTs simulation. Without an interactive but with a prescribed ocean, the enhanced damping reduces the variance in the atmosphere [*Barsugli and Battisti*, 1998].

In summary we find that for the tropospheric impact of major SSWs—a pattern which strongly projects on the NAO or AO and which lasts around 4 weeks—removing interannual SST variability and two-way ocean/atmosphere coupling seems to reduce the tropospheric signature in space and time. Removing the QBO seems to shift the period of significant influence by about 10 days.

6. Conclusions

In this study, we have investigated the influence of different natural and anthropogenic factors, namely, anthropogenic GHGs and ODSs, interannual SST variability, and the QBO, on major stratospheric warmings. For this, we have performed a set of sensitivity simulations with NCAR's CESM-WACCM model where we systematically switched on and off these factors, as summarized in Table 1. We analyzed differences in the frequency and distribution of major warmings and if these differences result from climatological differences in planetary wave generation, wave propagation, and wave-mean flow interaction. Afterward, we investigated the warming event itself, from its preconditioning phase until the downward coupling and surface impact afterward.

We found the following:

1. The frequency of major warmings is significantly increased by removing stratospheric variability provoked by the equatorial QBO, while it is significantly decreased when interannual SST variability and two-way atmosphere-ocean interaction is removed. These changes are consistent with differences in the climatological strength of the stratospheric polar night jet (PNJ) together with differences in climatological wave propagation and wave-mean flow interaction which, in turn, are all influenced by the QBO and SST variability. When QBO nudging is switched off and equatorial winds are in permanent easterly phase, planetary wave propagation from the troposphere into the PNJ region is enhanced, which leads to stronger deceleration of the PNJ through wave-mean flow interaction and, thus, to a weaker vortex that allows more major warmings to occur. Without SST variability, in contrast, the wave forcing from the troposphere is reduced, which means that the vortex is stronger and hence less easily disturbed.

Although the QBO and SST variability already have an influence on the generation of planetary waves in the troposphere, this does not seem to be the decisive factor for the differences in SSWs.

2. Anthropogenic GHGs and ODSs have some influence on the prewarming phase of the major warming events, i.e., the weeks before the central date. The GHG simulation shows an anomalous increase of the geopotential height wave 1 component starting several weeks before the warming, which does not occur in the other simulations where the GHGs are kept fixed at the 1960s level. In the simulation without anthropogenic forcing, a minor warming occurs in many cases around 5 weeks before the major warming, leading to a polar vortex which is already weakened before SSW occurrence.
3. In the phase following the central date, all experiments show a significant downward coupling to the troposphere and surface signature, which strongly projects on the negative NAO or AO pattern. It lasts around 4 weeks, probably due to the persistence of the signal in the ocean, but seems to be altered by the QBO and SST variability. Without the QBO, the 30 day period of significant surface influence is shifted by about 10 days. When the SSTs do not vary from year to year, the tropospheric signature seems to be confined to a smaller area (above the pole and the eastern North Atlantic) and a shorter period of time (between days 30 and 40 after the central date). This could be due to enhanced internal damping, which occurs when the ocean and atmosphere are not coupled interactively [*Barsugli and Battisti*, 1998]; however, this hypothesis has to be confirmed by future studies investigating more SSW cases, as the relatively low number of major warmings in the Fixed SSTs experiment does not allow final conclusions. The surface impact of major warmings in CESM-WACCM will not change significantly even under extreme (RCP8.5) global warming conditions.

Although many studies have reported a relationship between tropospheric blocking and the occurrence of major warmings, we can neither confirm nor negate this connection from our analysis, and we did not find any differences due to the different factors. However, this might be due to the inherent underestimation of Atlantic and Pacific blockings in the CESM model which has been documented for several models, e.g., in CMIP3 and CMIP5 [*Scaife et al.*, 2010; *Anstey et al.*, 2013], and which might be due to the relatively coarse horizontal resolution used in these models [*Jung et al.*, 2012]. Although the average amplitude and duration of major warmings does not seem to be influenced by the different factors, we found that SSWs preceded by a Euro-Atlantic blocking are on average longer than those which follow a Pacific blocking.

None of our simulations were able to reproduce the observed frequency of W2 and vortex split events; instead, almost all major warmings are W1 and vortex displacement warmings. This might also be due to the underestimation of blockings, as they (mainly the Pacific blockings) have been shown to often precede wave number 2 events.

With our study we confirm that all of the investigated factors influence several aspects of stratospheric warmings as described above; however, it is in general not easy to compare the effect of different factors directly, as they all influence atmospheric dynamics in different ways: the GHGs primarily act on the radiation budget, the QBO influences the dynamical stratospheric state, and the SSTs affect the lower to middle atmosphere from the lower boundary of the system. A subject of future studies is to deal with the quantification of the influence of the individual factors, e.g., by applying statistical methods. Knowledge about the absolute importance of the respective factors is crucial for the prediction of stratospheric polar vortex conditions and hence would increase the prediction skill for tropospheric weather.

Acknowledgments

This work has been performed within the Helmholtz-University Young Investigators Group NATHAN funded by the Helmholtz-Association through the President's Initiative and Networking Fund, the Helmholtz Centre for Ocean Research Kiel (GEOMAR), the German Centre for Geosciences Potsdam (GFZ), and the Freie Universität Berlin. The CESM simulations have been performed at the Deutsche Klimarechenzentrum (DKRZ) Hamburg, Germany. The authors thank D. Marsh, M. Mills, and the CESM development group at NCAR for help in setting up the coupled model at the DKRZ. Special thanks go to N.-E. Omrani, R. Thieblemont, and L. Neef for intensive discussions on the manuscript and to Shigeo Yoden and two anonymous reviewers for very helpful comments.

References

Andrews, D. G., J. Holton, and C. Leovy (1987), *Middle Atmosphere Dynamics*, Academic Press, San Diego, Calif.

Anstey, J. A., P. Davini, L. J. Gray, T. Woollings, N. Butchart, C. Cagnazzo, B. Christiansen, S. C. Hardiman, S. M. Osprey, and S. Yang (2013), Multi-model analysis of Northern Hemisphere winter blocking: Model biases and the role of resolution, *J. Geophys. Res. Atmos.*, *118*, 3956–3971, doi:10.1002/jgrd.50231.

Ayarzagüena, B., U. Langematz, S. Meul, S. Oberlander, J. Abalichin, and A. Kubin (2013), The role of climate change and ozone recovery for the future timing of major stratospheric warmings, *Geophys. Res. Lett.*, *40*, 2460–2465, doi:10.1002/grl.50477.

Baldwin, M., and T. Dunkerton (2001), Stratospheric harbingers of anomalous weather regimes, *Science*, *294*, 581–584.

Baldwin, M. P., and D. W. J. Thompson (2009), A critical comparison of stratosphere-troposphere coupling indices, *Q. J. R. Meteorol. Soc.*, *135*(644), 1661–1672, doi:10.1002/qj.479.

Bancala, S., K. Kruger, and M. Giorgetta (2012), The preconditioning of major sudden stratospheric warmings, *J. Geophys. Res.*, *117*, D04101, doi:10.1029/2011JD016769.

Barsugli, J. J., and D. S. Battisti (1998), The basic effects of atmosphere-ocean thermal coupling on midlatitude variability, *J. Atmos. Sci.*, *55*(4), 477–493, doi:10.1175/1520-0469(1998)055<0477:TBEOAO>2.0.CO;2.

Bell, C. J., L. J. Gray, A. J. Charlton-Perez, M. M. Joshi, and A. A. Scaife (2009), Stratospheric communication of El Nino teleconnections to European winter, *J. Clim.*, *22*(15), 4083–4096, doi:10.1175/2009JCLI2717.1.

Black, R. X., and B. A. McDaniel (2004), Diagnostic case studies of the northern annular mode, *J. Clim.*, *17*(20), 3990–4004, doi:10.1175/1520-0442(2004)017<3990:DCSOTN>2.0.CO;2.

Blume, C., K. Matthes, and I. Horenko (2012), Supervised learning approaches to classify sudden stratospheric warming events, *J. Atmos. Sci.*, *69*(6), 1824–1840, doi:10.1175/JAS-D-11-0194.1.

Butchart, N., J. Austin, J. R. Knight, A. A. Scaife, and M. L. Gallani (2000), The response of the stratospheric climate to projected changes in the concentrations of well-mixed greenhouse gases from 1992 to 2051, *J. Clim.*, *13*(13), 2142–2159, doi:10.1175/1520-0442(2000)013<2142:TROTSC>2.0.CO;2.

Butler, A. H., and L. M. Polvani (2011), El Niño, La Niña, and stratospheric sudden warmings: A reevaluation in light of the observational record, *Geophys. Res. Lett.*, *38*, L13807, doi:10.1029/2011GL048084.

Camp, C. D., and K. K. Tung (2007), Stratospheric polar warming by ENSO in winter: A statistical study, *Geophys. Res. Lett.*, *34*, L04809, doi:10.1029/2006GL028521.

Castanheira, J. M., and D. Barriopedro (2010), Dynamical connection between tropospheric blockings and stratospheric polar vortex, *Geophys. Res. Lett.*, *37*, L13809, doi:10.1029/2010GL043819.

Charlton, A. J., and L. M. Polvani (2007), A new look at stratospheric sudden warmings. Part I: Climatology and modeling benchmarks, *J. Clim.*, *20*(3), 449–469, doi:10.1175/JCLI3996.1.

Charlton, A. J., L. M. Polvani, J. Perlwitz, F. Sassi, E. Manzini, K. Shibata, S. Pawson, J. E. Nielsen, and D. Rind (2007), A new look at stratospheric sudden warmings. Part II: Evaluation of numerical model simulations, *J. Clim.*, *20*(3), 470–488, doi:10.1175/JCLI3994.1.

Charlton-Perez, A. J., L. M. Polvani, J. Austin, and F. Li (2008), The frequency and dynamics of stratospheric sudden warmings in the 21st century, *J. Geophys. Res.*, *113*, D16116, doi:10.1029/2007JD009571.

Danabasoglu, G., S. C. Bates, B. P. Briegleb, S. R. Jayne, M. Jochum, W. G. Large, S. Peacock, and S. G. Yeager (2012), The CCSM4 ocean component, *J. Clim.*, *25*(5), 1361–1389, doi:10.1175/JCLI-D-11-00091.1.

de la Torre, L., R. R. Garcia, D. Barriopedro, and A. Chandran (2012), Climatology and characteristics of stratospheric sudden warmings in the Whole Atmosphere Community Climate Model, *J. Geophys. Res.*, *117*, D04110, doi:10.1029/2011JD016840.

Erlebach, P., U. Langematz, and S. Pawson (1996), Simulations of stratospheric sudden warmings in the Berlin troposphere stratosphere mesosphere GCM, *Ann. Geophys.*, *14*(4), 443–463, doi:10.1007/s00585-996-0443-6.

Garcia, R. R., D. R. Marsh, D. E. Kinnison, B. A. Boville, and F. Sassi (2007), Simulation of secular trends in the middle atmosphere, 1950–2003, *J. Geophys. Res.*, *112*, D09301, doi:10.1029/2006JD007485.

Garcia, R. R., W. J. Randel, and D. E. Kinnison (2011), On the determination of age of air trends from atmospheric trace species, *J. Atmos. Sci.*, *68*(1), 139–154, doi:10.1175/2010JAS3527.1.

Garfinkel, C. I., A. H. Butler, D. W. Waugh, M. M. Hurwitz, and L. M. Polvani (2012), Why might stratospheric sudden warmings occur with similar frequency in El Nino and La Nina winters?, *J. Geophys. Res.*, *117*, D19106, doi:10.1029/2012JD017777.

Gent, P. R., et al. (2011), The Community Climate System Model Version 4, *J. Clim.*, *24*(19), 4973–4991, doi:10.1175/2011JCLI4083.1.

Gray, L. J., et al. (2010), Solar influences on climate, *Rev. Geophys.*, *48*, RG4001, doi:10.1029/2009RG000282.

Hansen, F., K. Matthes, and L. J. Gray (2013), Sensitivity of stratospheric dynamics and chemistry to QBO nudging width in the chemistry-climate model WACCM, *J. Geophys. Res. Atmos.*, *118*, 10,464–10,474, doi:10.1002/jgrd.50812.

Holland, M. M., D. A. Bailey, B. P. Briegleb, B. Light, and E. Hunke (2012), Improved sea ice shortwave radiation physics in CCSM4: The impact of melt ponds and aerosols on Arctic Sea ice, *J. Clim.*, *25*(5), 1413–1430, doi:10.1175/JCLI-D-11-00078.1.

Holton, J. R., and H.-C. Tan (1980), The influence of the equatorial quasi-biennial oscillation on the global circulation at 50 mb, *J. Atmos. Sci.*, *37*, 2200–2208.

Holton, J. R., and H.-C. Tan (1982), The quasi-biennial oscillation in the Northern Hemisphere lower stratosphere, *J. Meteorol. Soc. Jpn.*, *60*, 140–148.

Huebener, H., U. Cubasch, U. Langematz, T. Spangehl, F. Niehorster, I. Fast, and M. Kunze (2007), Ensemble climate simulations using a fully coupled ocean-troposphere-stratosphere general circulation model, *Philos. Trans. R. Soc. A*, *365*(1857), 2089–2101, doi:10.1098/rsta.2007.2078.

Hurrell, J. W., et al. (2013), The Community Earth System Model: A framework for collaborative research, *Bull. Am. Meteorol. Soc.*, *94*(9), 1339–1360, doi:10.1175/BAMS-D-12-00121.1.

Jung, T., et al. (2012), High-resolution global climate simulations with the ECMWF Model in Project Athena: Experimental design, model climate, and seasonal forecast skill, *J. Clim.*, *25*(9), 3155–3172, doi:10.1175/JCLI-D-11-00265.1.

Kinnison, D. E., et al. (2007), Sensitivity of chemical tracers to meteorological parameters in the MOZART-3 chemical transport model, *J. Geophys. Res.*, *112*, D20302, doi:10.1029/2006JD007879.

Kodera, K., and M. Chiba (1995), Tropospheric circulation changes associated with stratospheric sudden warmings—A case study, *J. Geophys. Res.*, *100*(D6), 11,055–11,068, doi:10.1029/95JD00771.

Kolstad, E. W., and A. J. Charlton-Perez (2011), Observed and simulated precursors of stratospheric polar vortex anomalies in the Northern Hemisphere, *Clim. Dyn.*, *37*(7–8), 1443–1456, doi:10.1007/s00382-010-0919-7.

Labitzke, K. (1977), Interannual variability of the winter stratosphere in Northern Hemisphere, *Mon. Weather Rev.*, *105*, 762–770.

Labitzke, K., and B. Naujokat (2000), The lower Arctic stratosphere in winter since 1952, *SPARC Newsletter*, *15*, 11–14.

Lean, J. L., G. Rottman, J. Harder, and G. Kopp (2005), Source contributions to new understanding of global change and solar variability, *Sol. Phys.*, *230*, 27–53.

Limpasuvan, V., D. W. J. Thompson, and D. L. Hartmann (2004), The life cycle of the Northern Hemisphere sudden stratospheric warmings, *J. Clim.*, *17*(13), 2584–2596, doi:10.1175/1520-0442(2004)017<2584:TLCOTN>2.0.CO;2.

Limpasuvan, V., J. H. Richter, Y. J. Orsolini, F. Stordal, and O. K. Kvissel (2012), The roles of planetary and gravity waves during a major stratospheric sudden warming as characterized in WACCM, *J. Atmos. Sol. Terr. Phys.*, *78-79*, 84–98, doi:10.1016/j.jastp.2011.03.004.

Manzini, E., M. A. Giorgetta, M. Esch, L. Kornblueh, and E. Roeckner (2006), The influence of sea surface temperatures on the northern winter stratosphere: Ensemble simulations with the MAECHAM5 model, *J. Clim.*, *19*(16), 3863–3881, doi:10.1175/JCLI3826.1.

Marsh, D., M. J. Mills, D. E. Kinnison, J.-F. Lamarque, N. Calvo, and L. M. Polvani (2013), Climate change from 1850 to 2005 simulated in CESM1(WACCM), *J. Clim.*, *26*, 7372–7391, doi:10.1175/JCLI-D-12-00558.1.

Martius, O., L. M. Polvani, and H. C. Davies (2009), Blocking precursors to stratospheric sudden warming events, *Geophys. Res. Lett.*, *36*, L14806, doi:10.1029/2009GL038776.

Matsuno, T. (1971), Dynamical model of stratospheric sudden warming, *J. Atmos. Sci.*, *28*(8), 1479–1494, doi:10.1175/1520-0469(1971)028<1479:ADMOTS>2.0.CO;2.

Matthes, K., D. R. Marsh, R. R. Garcia, D. E. Kinnison, F. Sassi, and S. Walters (2010), Role of the QBO in modulating the influence of the 11 year solar cycle on the atmosphere using constant forcings, *J. Geophys. Res.*, *115*, D18110, doi:10.1029/2009JD013020.

Matthes, K., K. Kodera, R. R. Garcia, Y. Kuroda, D. R. Marsh, and K. Labitzke (2013), The importance of time-varying forcing for QBO modulation of the atmospheric 11 year solar cycle signal, *J. Geophys. Res. Atmos.*, *118*, 4435–4447, doi:10.1002/jgrd.50424.

McLandress, C., and T. G. Shepherd (2009), Impact of climate change on stratospheric sudden warmings as simulated by the Canadian Middle Atmosphere Model, *J. Clim.*, *22*(20), 5449–5463, doi:10.1175/2009JCLI3069.1.

Meinshausen, M., et al. (2011), The RCP greenhouse gas concentrations and their extensions from 1765 to 2300, *Clim. Change*, *109*(1–2), 213–241, doi:10.1007/s10584-011-0156-z.

Mitchell, D. M., A. J. Charlton-Perez, and L. J. Gray (2011), Characterizing the variability and extremes of the stratospheric polar vortices using 2D moment analysis, *J. Atmos. Sci.*, *68*(6), 1194–1213, doi:10.1175/2010JAS3555.1.

Mitchell, D. M., S. M. Osprey, L. J. Gray, N. Butchart, S. C. Hardiman, A. J. Ciarlton-Perez, and P. Watson (2012), The effect of climate change on the variability of the Northern Hemisphere stratospheric polar vortex, *J. Atmos. Sci.*, *69*(8), 2608–2618, doi:10.1175/JAS-D-12-021.1.

Mitchell, D. M., L. J. Gray, J. Anstey, M. P. Baldwin, and A. J. Charlton-Perez (2013), The influence of stratospheric vortex displacements and splits on surface climate, *J. Clim.*, *26*(8), 2668–2682, doi:10.1175/JCLI-D-12-00030.1.

Naoe, H., and K. Shibata (2010), Equatorial quasi-biennial oscillation influence on northern winter extratropical circulation, *J. Geophys. Res.*, *115*, D19102, doi:10.1029/2009JD012952.

Nishii, K., H. Nakamura, and Y. J. Orsolini (2011), Geographical dependence observed in blocking high influence on the stratospheric variability through enhancement and suppression of upward planetary-wave propagation, *J. Clim.*, *24*(24), 6408–6423, doi:10.1175/JCLI-D-10-05021.1.

Omrani, N. E., N. S. Keenlyside, J. Bader, and E. Manzini (2014), Stratosphere key for wintertime atmospheric response to warm Atlantic decadal conditions, *Clim. Dyn.*, *42*(3–4), 649–663, doi:10.1007/s00382-013-1860-3.

Pawson, S., and T. Kubitz (1996), Climatology of planetary waves in the northern stratosphere, *J. Geophys. Res.*, *101*(D12), 16,987–16,996, doi:10.1029/96JD01226.

Quiroz, R. S. (1977), Tropospheric-stratospheric polar vortex breakdown of January 1977, *Geophys. Res. Lett.*, *4*(4), 151–154, doi:10.1029/GL004i004p00151.

Quiroz, R. S. (1986), The association of stratospheric warmings with tropospheric blocking, *J. Geophys. Res.*, *91*(D4), 5277–5285, doi:10.1029/JD091iD04p05277.

Richter, J. H., F. Sassi, and R. R. Garcia (2010), Toward a physically based gravity wave source parameterization in a general circulation model, *J. Atmos. Sci.*, *67*(1), 136–156, doi:10.1175/2009JAS3112.1.

Richter, J. H., K. Matthes, N. Calvo, and L. J. Gray (2011), Influence of the quasi-biennial oscillation and El Niño-Southern Oscillation on the frequency of sudden stratospheric warmings, *J. Geophys. Res.*, *116*, D20111, doi:10.1029/2011JD015757.

Rind, D., D. Shindell, P. Lonergan, and N. K. Balachandran (1998), Climate change and the middle atmosphere. Part III: The doubled CO_2 climate revisited, *J. Clim.*, *11*(5), 876–894, doi:10.1175/1520-0442(1998)011<0876:CCATMA>2.0.CO;2.

Robock, A. (2000), Volcanic eruptions and climate, *Rev. Geophys.*, *38*(2), 191–219, doi:10.1029/1998RG000054.

Sassi, F., D. Kinnison, B. A. Boville, R. R. Garcia, and R. Roble (2004), Effect of El Niño-Southern Oscillation on the dynamical, thermal, and chemical structure of the middle atmosphere, *J. Geophys. Res.*, *109*, D17108, doi:10.1029/2003JD004434.

Scaife, A. A., T. Woollings, J. Knight, G. Martin, and T. Hinton (2010), Atmospheric blocking and mean biases in climate models, *J. Clim.*, *23*(23), 6143–6152, doi:10.1175/2010JCLI3728.1.

Scherhag, R. (1952), Die explosionsartigen Stratosphärenerwärmungen des Spätwinters, 1951-1952, *Ber. Deut. Wetterdienst*, *38*, 51–63.

Schimanke, S., J. Korper, T. Spangehl, and U. Cubasch (2011), Multi-decadal variability of sudden stratospheric warmings in an AOGCM, *Geophys. Res. Lett.*, *38*, L01801, doi:10.1029/2010GL045756.

Schimanke, S., T. Spangehl, H. Huebener, and U. Cubasch (2013), Variability and trends of major stratospheric warmings in simulations under constant and increasing GHG concentrations, *Clim. Dyn.*, *40*(7-8), 1733–1747, doi:10.1007/s00382-012-1530-x.

Shepherd, T. G., and C. Mclandress (2011), A robust mechanism for strengthening of the Brewer-Dobson circulation in response to climate change: Critical-layer control of subtropical wave breaking, *J. Atmos. Sci.*, *68*(4), 784–797, doi:10.1175/2010JAS3608.1.

Simmons, A. J., S. M. Uppala, D. Dee, and S. Kobayashi (2006), ERA-Interim: New ECMWF reanalysis products from 1989 onwards, *ECMWF Newsletter*, *110*, 26–35.

Smith, A. K., R. R. Garcia, D. R. Marsh, and J. H. Richter (2011), WACCM simulations of the mean circulation and trace species transport in the winter mesosphere, *J. Geophys. Res.*, *116*, D20115, doi:10.1029/2011JD016083.

SPARC CCMVal, (2010), SPARC report on the evaluation of chemistry-climate models, *SPARC-Report No. 5, WCRP-132,WMO/TD-No. 1526*, SPARC CCMVal.

Taguchi, M. (2008), Interannual variations of the stratosphere and troposphere during northern winter as simulated by WACCM, *J. Clim.*, *21*(10), 2326–2331, doi:10.1175/2007JCLI1744.1.

Taguchi, M., and D. L. Hartmann (2006), Increased occurrence of stratospheric sudden warmings during El Niño as simulated by WACCM, *J. Clim.*, *19*(3), 324–332, doi:10.1175/JCLI3655.1.

Taylor, K., R. J. Stouffer, and G. A. Meehl (2012), An overview of CMIP5 and the experiment design, *Bull. Am. Meteorol. Soc.*, *93*, 485–498.

Thompson, D., and J. Wallace (1998), The Arctic Oscillation signature in the wintertime geopotential height and temperature fields, *Geophys. Res. Lett.*, *25*(9), 1297–1300, doi:10.1029/98GL00950.

Thompson, D. W. J., M. P. Baldwin, and J. M. Wallace (2002), Stratospheric connection to Northern Hemisphere wintertime weather: Implications for prediction, *J. Clim.*, *15*(12), 1421–1428, doi:10.1175/1520-0442(2002)015<1421:SCTNHW>2.0.CO;2.

Tibaldi, S., and F. Molteni (1990), On the operational predictability of blocking, *Tellus Ser. A*, *42*, 343–365.

Uppala, S., P. Kallberg, P. Hernandez, S. Saarinen, M. Fiorino, X. Li, K. Onogi, N. Sokka, U. Andrae, and V. D. C. Bechtold (2004), ERA-40: ECMWF 45-year reanalysis of the global atmosphere and surface conditions 1957–2002, *ECMWF Newsletter*, *101*, 2–21.

Van Loon, H., and K. Labitzke (1987), The Southern Oscillation .5. The anomalies in the lower stratosphere of the Northern-Hemisphere in winter and a comparison with the Quasi-biennial Oscillation, *Mon. Weather Rev.*, *115*(2), 357–369, doi:10.1175/1520-0493(1987)115<0357:TSOPVT>2.0.CO;2.

Wallace, J. M., and D. S. Gutzler (1981), Teleconnections in the geopotential height field during the Northern Hemisphere winter, *Mon. Weather Rev.*, *109*(4), 784–812, doi:10.1175/1520-0493(1981)109<0784:TITGHF>2.0.CO;2.

Watson, P. A. G., and L. J. Gray (2014), How does the quasi-biennial oscillation affect the stratospheric polar vortex?, *J. Atmos. Sci.*, *71*(1), 391–409, doi:10.1175/JAS-D-13-096.1.

Woollings, T., A. Charlton-Perez, S. Ineson, A. G. Marshall, and G. Masato (2010), Associations between stratospheric variability and tropospheric blocking, *J. Geophys. Res.*, *115*, D06108, doi:10.1029/2009JD012742.

Yoden, S., T. Yamaga, S. Pawson, and U. Langematz (1999), A composite analysis of the stratospheric sudden warmings simulated in a perpetual January integration of the Berlin TSM GCM, *J. Meteorol. Soc. Jpn.*, *77*(2), 431–445.